Event-based Bispectral Photometry using Temporally Modulated Illumination*

Tsuyoshi Takatani† Yuzuha Ito† Ayaka Ebisu† Yinqiang Zheng‡ Takahito Aoto†

†University of Tsukuba, Japan ‡The University of Tokyo, Japan

Abstract

Analysis of bispectral difference plays a critical role in various applications that involve rays propagating in a light absorbing medium. In general, the bispectral difference is obtained by subtracting signals at two individual wavelengths captured by ordinary digital cameras, which tends to inherit the drawbacks of conventional cameras in dynamic range, response speed and quantization precision. In this paper, we propose a novel method to obtain a bispectral difference image using an event camera with temporally modulated illumination. Our method is rooted in a key observation on the analogy between the bispectral photometry principle of the participating medium and the event generating mechanism in an event camera. By carefully modulating the bispectral illumination, our method allows to read out the bispectral difference directly from triggered events. Experiments using a prototype imaging system have verified the feasibility of this novel usage of event cameras in photometry based vision tasks, such as 3D shape reconstruction in water.

1. Introduction

Analysis of bispectral difference, *i.e.* difference of the absorbance between two individual wavelengths, plays a critical role in various applications that involve rays propagating in a light absorbing medium, such as water. Since the absorbance of a medium depends on the wavelength of light and the medium itself, bispectral analysis of the absorbance allows to determine some quantities that might serve various purposes. For example, in analytical chemistry, a relative concentration of matter in a mixture is determined from the bispectral difference [41], and in atmospheric science, analysis of the bispectral difference is employed to trace and classify gasses and particles [23].

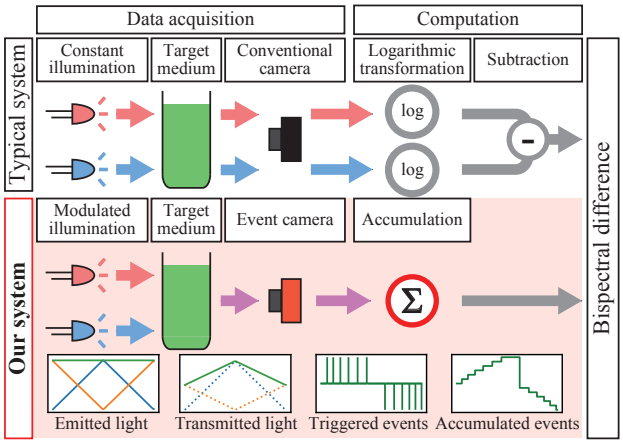

Figure 1: Abstract of our method. Our system allows to read out the bispectral difference directly as the number of events triggered by the temporally modulated illumination, in which the operations required in the typical system are conducted by the event camera.

In general, the bispectral difference is obtained by subtracting signals at the two wavelengths captured by ordinary digital cameras. A typical system of bispectral photometry uses a conventional camera, as shown in Fig. 1 (top). Light at the two wavelengths illuminates a target medium and then the camera captures transmitted light at each of the wavelengths. The logarithms of the captured signals and the subtraction of them result in the bispectral difference. Although the operations in themselves are not complicated, the performance of obtaining the bispectral difference is affected by the well-known drawbacks of conventional cameras in dynamic range and quantization precision essentially. Thus, a specific system is required to resolve these problems.

Recently, event cameras have emerged in robotics and computer vision. Event cameras do not capture brightness images at a fixed rate. Instead, each pixel inside an event camera independently and asynchronously records a tem-

*This work was partially supported by JSPS KAKENHI Grant Numbers JP20H04215, JP20H05951 and JP17H04686. It has been conducted when T. Takatani and Y. Zheng were affiliated with National Institute of Informatics, Japan. The corresponding author is Y. Zheng (yqzheng@ai.u-tokyo.ac.jp).

poral change in brightness as an event. Compared to conventional cameras, event cameras have superior features of high dynamic range (HDR), high temporal resolution, and low power consumption. Furthermore, event cameras have remarkable features inside their electronic circuit, which have not been deeply delved. In event cameras, first, a light signal is logarithmically amplified [22, 35]. And then the signal is temporally differentiated. Finally, an event is triggered when the difference reaches a threshold (Fig. 2). This mechanism is analogous to the operations in the typical system.

In this paper, we propose a novel method to obtain a bispectral difference image using an event camera with temporally modulated illumination, as shown in Fig. 1 (bottom). Temporally modulated light at two individual wavelengths illuminates a target medium. The event camera records a temporal series of events triggered by the modulated bispectral illumination. The bispectral difference is read out directly as the number of the events because the operations required in the typical system are conducted by the event camera. We develop a prototype imaging system and validate our method in real experiments on depth recovery in water and turbid medium concentration estimation.

This paper has three major contributions. First, we discover an interesting analogy between the bispectral photometry principle of the participating medium and the event generating mechanism in an event camera. Second, by carefully modulating the bispectral illumination, our method allows to read out the bispectral difference directly as the number of events. Third, the experiments verify the feasibility of the novel usage of event cameras in photometry based vision tasks, such as 3D shape reconstruction in water.

2. Related work

2.1. Bispectral photometry

Bispectral photometry, proposed by Chance [8], uses two individual wavelengths in spectral photometry which analyzes exponentially decayed light, unlike traditional spectrophotometry using a single wavelength. While the traditional spectrophotometry can handle a transparent medium only, the bispectral photometry can handle a turbid medium [11]. The bispectral photometry obtains a bispectral difference and analysis of the bispectral difference allows to determine some quantities of a medium. The bispectral photometry plays an important role in various fields. In analytical chemistry, the relative concentration or amount of matter in a mixture is determined from the bispectral difference [41, 51, 31, 17]. In atmospheric science, the bispectral difference is often used to trace and classify particles and gases [10, 23, 21, 26, 34], estimate cloud parameters [37], and determine the amount of water vapor in air [13, 49]. In medical science, analysis of the bispectral difference is applied for determining the concentration of hemoglobin in blood [45], assaying chemicals [18, 16], estimating the water concentration in human cornea [33], and improving imaging with optical coherence tomography [38, 47]. In computer vision, the bispectral difference also allows to reconstruct the 3D shape of an object in a known medium [6, 3]. Basically, the bispectral photometry employs ordinary digital cameras with the operations, as described in Fig. 1 (top), or a single pixel probe including an analog logarithmic amplifier which requires scanning to obtain a bispectral difference image. On the other hand, our method using an event camera, whose each pixel includes analog logarithmic amplifier and differentiator, can obtain a bispectral difference image based on the analogy between the bispectral photometry principle and the event generating mechanism.

2.2. Event-based methods

Event cameras, such as Dynamic Vision Sensor [22] and Asynchronous Time-based Image Sensor [35], independently and asynchronously record temporal changes in brightness as events on each pixel. In robotics and computer vision, event cameras have been applied to detect and track feature points for object tracking [9, 15, 27], visual odometry [52, 5], 3D reconstruction [39, 2, 53], and simultaneous localization and mapping (SLAM) [19]. In order to apply event cameras for conventional computer vision techniques, such as classification [42], there have also been a lot of work to reconstruct a brightness image [4, 24, 29] or a video [32, 36] from events. These methods also achieve reconstruction of HDR and high-speed video frames which cannot be captured by conventional cameras [48]. Recently, recognitional tasks have been handled with event cameras. Since event cameras do not capture a brightness image, as described above, conventional deep learning techniques based on images cannot be directly applied for event data. In response, event-based learning using sparse event sequences [46, 40, 14] have ably managed the event data. These event-based methods rely on the well known features of event cameras: HDR, high temporal resolution, and low power consumption. However, event cameras also have other remarkable features inside their electronic circuit, which have not been deeply delved. This work is the first challenge to bring out the hidden features towards the novel usage of event cameras in photometry based analysis.

2.3. Temporal synchronization

In general, active sensing systems require temporal synchronization between sensors and light sources. A major system based on the temporal synchronization is Time-of-flight (ToF) cameras which are often used for obtaining depth images [28, 1]. ToF cameras read out correlations

between emitted and reflected light signals under temporally modulated illumination. Each pixel inside a ToF camera has multiple capacitors, synchronized to the modulated light signals. The capacitors store electric charges individually at different times. Another application using ToF camera is material analysis, such as material classification using distorted temporal correlations due to subsurface scattering [44] and visualization of spectral difference using temporally modulated multispectral illumination [20]. Also, a ToF camera with temporally modulated bispectral illumination allows to discriminate the dichroism in a scene, such as red and blue [7]. However, each pixel inside a ToF camera differentiates signals in analog form without logarithmic amplifiers. ToF cameras are, therefore, not applicable to the bispectral photometry requiring logarithmic operations. Instead, event cameras are applicable by using temporally modulated illumination.

Another major system based on the temporal synchronization is structured light systems, such as [30]. While a projector illuminates a scene with structured patterns, a camera captures the scene. Structured light systems are often used for 3D shape reconstruction and light transport analysis. There has been a structured light method using an event camera with laser scanning [25]. This method relies on the well known features of event cameras, such as HDR and high temporal resolution, to reconstruct the 3D shape of highly dynamic objects under strong ambient illumination. On the other hand, this work brings out the hidden features inside an event camera and utilizes them for photometry based analysis.

3. Preliminaries

3.1. Bispectral photometry principle

According to the Beer-Lambert law [43], light intensity transmitted through a medium follows an exponential decay, as below;

$$L_o(\lambda) = L_i(\lambda)\exp(-\alpha(\lambda)), \tag{1}$$

where λ denotes a wavelength of light, $L_i(\lambda)$ and $L_o(\lambda)$ are incident and outgoing light intensities at the wavelength, respectively, and $\alpha(\lambda)$ is the spectral absorbance of the medium. The spectral absorbance is determined with an extinction cross section $\mu(\lambda)$, a number concentration c of the medium, and an optical path length l, as below;

$$\alpha(\lambda) = \mu(\lambda)cl. \tag{2}$$

A bispectral difference $\Delta\alpha(\lambda_1, \lambda_2)$, which is a difference of the absorbances between two individual wavelengths λ_1 and λ_2, is calculated from Eq. (1), as follows;

$$\begin{aligned}\Delta\alpha(\lambda_1, \lambda_2) &= \alpha(\lambda_1) - \alpha(\lambda_2) &(3)\\ &= \ln L_o(\lambda_2) - \ln L_o(\lambda_1), &(4)\end{aligned}$$

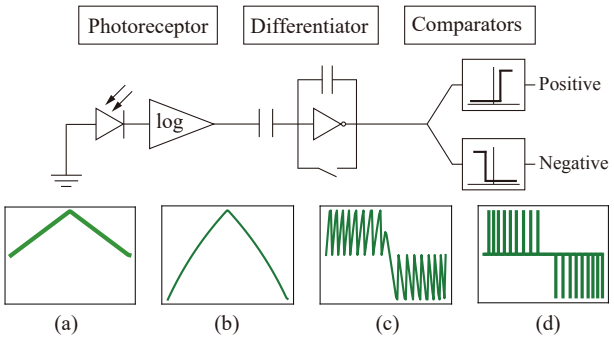

Figure 2: Electronic circuit of each pixel inside an event camera. (a) Received light in the time domain. (b) Logarithmically amplified signal. (c) Differential signal with resets. (d) Triggered events.

where the incident light intensities at both the wavelengths are assumed to be identical, *e.g.*, $L_i(\lambda_1) = L_i(\lambda_2)$. A relationship is derived from Eq. (2) and Eq. (3), as below;

$$\begin{aligned}\Delta\alpha(\lambda_1, \lambda_2) &= (\mu(\lambda_1) - \mu(\lambda_2))cl &(5)\\ &= \mathrm{L}c &(6)\\ &= \mathrm{C}l, &(7)\end{aligned}$$

where $\mathrm{L} \coloneqq (\mu(\lambda_1) - \mu(\lambda_2))l$ and $\mathrm{C} \coloneqq (\mu(\lambda_1) - \mu(\lambda_2))c$. In analytical chemistry, once the constant L is determined with a known optical path length, such as a cuvette size, the concentration c in mixture solution can be reconstructed from Eq. (6). Also, once the constant C is determined with a known concentration, such as water, the optical path length l can be reconstructed from Eq. (7), which has been applied for 3D shape reconstruction in water.

3.2. Event generating mechanism

The electronic circuit of each pixel inside an event camera mainly consists of three parts [22, 35]: photoreceptor, differentiator, and comparators, as shown in Fig. 2. The photoreceptor converts light into an electrical signal with logarithmic amplification, as shown in Fig. 2 (left). This is expressed as below;

$$S_a(\boldsymbol{x}, t) = \ln S_p(\boldsymbol{x}, t), \tag{8}$$

where $S_p(\boldsymbol{x}, t)$ denotes the electrical signal at a pixel $\boldsymbol{x}$ at a time t and $S_a(\cdot)$ is the amplified signal. The differentiator calculates a temporal difference. It consists of a capacitor and an integral circuit, as shown in Fig. 2 (middle). The capacitor differentiates the amplified signal and the integral circuit accumulates it. The integral circuit is reset when comparators triggers an event. Thus, a differential signal $\Delta S_a(\cdot)$ output from the differentiator is expressed as below;

$$\begin{aligned}\Delta S_a(\boldsymbol{x}, t) &= S_a(\boldsymbol{x}, t) - S_a(\boldsymbol{x}, \tau(t)) &(9)\\ &= \ln S_p(\boldsymbol{x}, t) - \ln S_p(\boldsymbol{x}, \tau(t)), &(10)\end{aligned}$$

where $\tau(t)$ denotes a time when the previous event is triggered before the time t. The comparators trigger a positive or negative event, when the differential signal gets over thresholds, as shown in Fig. 2 (right). The thresholds for the positive and negative events are assumed to be identical in this paper. This thresholding is formulated by a ternarization function, as below;

$$\mathcal{T}(\Delta S_a(\boldsymbol{x},t),h) = \begin{cases} +1, & \Delta S_a(\boldsymbol{x},t) \geq h \\ 0, & \Delta S_a(\boldsymbol{x},t) \in (-h,h) \\ -1, & \Delta S_a(\boldsymbol{x},t) \leq -h \end{cases} \quad (11)$$

where h is the threshold whether to trigger an event.

4. Event-based bispectral photometry

We propose event-based bispectral photometry to obtain a bispectral difference image using an event camera with temporally modulated illumination, as shown in Fig. 1 (bottom). The key observation is the analogy between the bispectral photometry principle of the participating medium, as described in Eq. (4), and the event generating mechanism in an event camera. It is required for the temporal difference, as described in Eq. (10), to be converted into a spectral difference via temporally modulated bispectral illumination so that the event camera allows to read out the bispectral difference.

4.1. Design of temporally modulated illumination

An illumination module emits light at two individual wavelengths λ_1 and λ_2, and their modulation functions are indicated as $f_1(t)$ and $f_2(t)$, respectively. The modulation functions are assumed to be cyclic functions, such as sinusoidal and triangle waves, and satisfy conditions;

$$f_1(t), f_2(t) \geq 0 \quad \forall t \in [0,T), \quad (12)$$
$$f_1(t) + f_2(t) = 1 \quad \forall t \in [0,T), \quad (13)$$
$$f_1(t) = 0 \quad \exists t \in [0,T), \quad (14)$$
$$f_2(t) = 0 \quad \exists t \in [0,T), \quad (15)$$

where T denotes a temporal period of the modulation functions. The total incident light intensity $I_i(t)$ for both the wavelengths at a time t into an medium is expressed as follows;

$$I_i(t) = L_i(\lambda_1) f_1(t) + L_i(\lambda_2) f_2(t). \quad (16)$$

According to Eqs. (1) and (16), light transmitted through the medium is expressed as follows;

$$I_o(t) = L_i(\lambda_1)\exp(-\alpha(\lambda_1)) f_1(t) + L_i(\lambda_2)\exp(-\alpha(\lambda_2)) f_2(t), \quad (17)$$

where $I_o(t)$ denotes the total outgoing light intensity. Once a modulation function for a wavelength is designed, the other function is automatically determined from Eq. (13). There are two important times in the modulation functions;

$$\exists t_1 \in [0,T) \quad \text{s.t.} \quad f_1(t) = 1, f_2(t) = 0, \quad (18)$$
$$\exists t_2 \in [0,T) \quad \text{s.t.} \quad f_1(t) = 0, f_2(t) = 1, \quad (19)$$

according to the conditions, Eqs. (13)-(15). At these times, the outgoing light is expected as;

$$t = t_1 \rightarrow I_o(t_1) = L_o(\lambda_1), \quad (20)$$
$$t = t_2 \rightarrow I_o(t_2) = L_o(\lambda_2). \quad (21)$$

4.2. Reconstruction of bispectral difference

The outgoing light is received by the event camera, which records events triggered by its temporal change, as;

$$S_p(t) = I_o(t), \quad (22)$$

in Eqs. (8)-(11). For simplicity, we omit the pixel location $\boldsymbol{x}$ and it is assumed that the spectral sensitivity of the event camera at both the wavelengths is identical in this formulation. However, in actual, the spectral sensitivity is not flat, and thus, a practical way to calibrate that is explained in Sec. 5.1. From Eqs. (4), (8) and (20)-(22), the bispectral difference can be expressed as;

$$\Delta\alpha(\lambda_1,\lambda_2) = S_a(t_2) - S_a(t_1). \quad (23)$$

As described in Sec. 3.2, an event is triggered every time when a temporal change in the amplified signal gets over the threshold h. Thus, accumulating the triggered events in the duration from t_1 to t_2 allows to reconstruct the bispectral difference, as follows;

$$\Delta\alpha(\lambda_1,\lambda_2) = \int_{t=t_1}^{t_2} \Delta S_a(t) dt \quad (24)$$
$$\simeq \int_{t=t_1}^{t_2} h\mathcal{T}(\Delta S_a(t),h) dt \quad (25)$$
$$= h(n_p - n_n), \quad (26)$$

where n_p and n_n are the number of positive and negative events in the duration. If the modulation function is designed as a monotonically increasing function in the duration, the triggered events are positive only, *e.g.*, $n_n = 0$, and the error of the reconstructed bispectral difference lies in $(-h,h)$, theoretically.

4.3. Shape reconstruction

The bispectral difference can be applied for 3D shape reconstruction [3]. Both the event camera and the illumination module are closely located as aiming at the same direction and a target object is sunk in a medium, as shown in Fig. 3. Emitted light penetrates the medium, reflects off

the object, and comes back to the camera. In this setup, the outgoing light intensity is re-formulated as below;

$$L_o(\lambda) = g(\omega)r(\lambda)L_i(\lambda)\exp(-\alpha(\lambda)), \tag{27}$$

where, $g(\omega)$ denotes the geometric characteristic of a surface of the object for a solid angle ω and $r(\lambda)$ is the reflectance of the surface at a wavelength λ. The geometric characteristic does not depend on the wavelength of light. The wavelengths λ_1 and λ_2 are carefully selected such that the reflectances at both the wavelengths are assumed to be almost identical, *e.g.*, $r(\lambda_1) \simeq r(\lambda_2)$. The incident light intensities at both the wavelengths are assumed to be identical, *e.g.*, $L_i(\lambda_1) = L_i(\lambda_2)$. According to Eqs. (4), (7), (26) and (27), a distance to the object d is calculated as follows;

$$d = \frac{h(n_p - n_n)}{2\mathrm{C}}, \tag{28}$$

because the light makes a round trip from the system to the object.

5. Experiments

5.1. Implementation

We implement a prototype imaging system with an event camera (Prophesee EVK or iniVation DVS346) and an illumination module consists of two light sources, as shown in Fig. 3. The light sources are collocated to illuminate a scene uniformly using a beam combiner. As the light sources, we use laser diodes at wavelengths of 915 and 940 nm (QPhotonics QLD-915-200S and QLD-940-200S, respectively) for reconstructing distances and shape in water. The wavelengths were so selected that reflectances of target materials at both the wavelengths are regarded as almost identical, referred to the work by Asano et al. [3]. Modulation signals to the illumination module are generated by a signal generator (Rigol DG4062), which also outputs synchronization signals to the event camera. In experiments with the typical system, we replace the event camera with a conventional camera (FLIR BFS-U3-51S5M-C). In all experiments in this paper, we use triangle waves as the modulation signals because it is reasonably efficient to generate the opposite modulation signal by phase shifting, and it is a monotonically increasing or decreasing function in a half of its period. Since the incident light intensities are proportional to the amplitudes of the waves, they have to be adjusted depending on components in the system. The frequency of the waves is a considerable factor affecting the performance of our method, which will be discussed in Sec. 6.1.

In the experiments in water, a glass tank (GEX Glassterior Cube) is filled with water. The system is also supposed to be sunk in water but there is less space in the tank and the devices are not water-proof. Thus, we set the system out

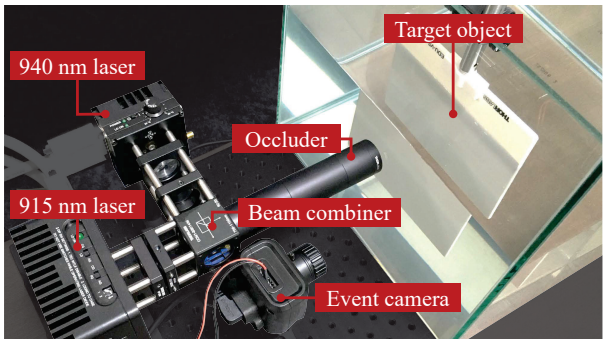

Figure 3: Experimental setup. The occluder is used to suppress direct specular reflection from the glass wall.

of the tank. Although refraction of light on the boundaries among air, glass, and water changes the optical path length, it is geometrically calibrated before all the experiments as well as [30]. Since the spectral sensitivity of the event camera is not provided and it is not obvious to measure that, we perform photometric calibration within the whole system. In a setup, a spectral standard (X-Rite ColorChecker) is placed in the glass tank without water and then the amplitudes of the modulation signals are adjusted such that no events is triggered under the modulated illumination. This process spectrally calibrates the system including the illumination module, the glass tank and the sensitivity of the event camera. Also, the typical system using the conventional camera is similarly calibrated such that captured intensities of the spectral standard are identical under constant illumination with each of the light sources.

5.2. Validation

We validate that our method allows to obtain the bispectral difference using the Prophesee EVK. First, we analyze recorded events when a white board is sunk in water at a distance of 100 mm from the wall of the glass tank. The frequency of the modulation signals is set to 10 Hz. The recorded events show that positive events are mainly recorded during a half of the period while negative events are done during another half, as shown in Fig. 4. We record events for 100 periods of the modulation signals and calculate the average and standard deviation of the number of recorded positive events per a half of the period, resulting in 42.0 and 2.1, respectively.

Next, we linearly translate the white board every 10 mm in a range between 10 and 250 mm. As explained in Eq. (28), the bispectral difference is proportional to the distance. Figure 5 shows the average number of positive events with its standard deviation as a vertical bar per a half of the period at each distance. In the range of the distance from 10 to 100 mm, the average number of events tends to be linearly proportional to the distance. Thus, in that range, the proposed method can properly obtain the bispectral differ-

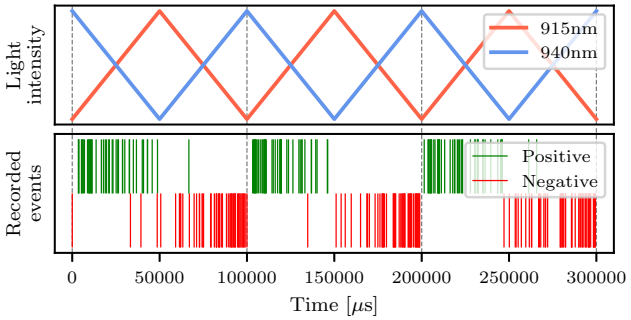

Figure 4: Temporal series of recorded events under the bispectral illumination modulated by triangle waves. The frequency of the triangle waves is set to 10 Hz.

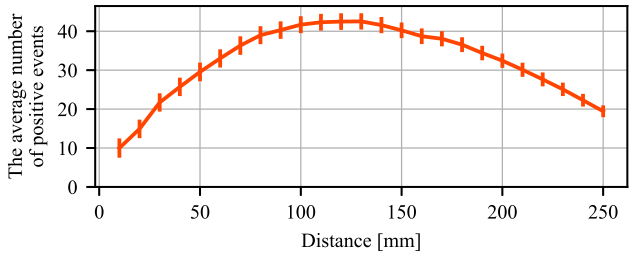

Figure 5: The average number of positive events per a half of the period at different distances to the white board. The events were recorded for 100 periods of the modulation signals. The vertical bar at each point is the range of one sigma for the 100 measurements.

ence. However, in the range over 110 mm, the average number is neither linear nor proportional to the distance. This is because light at one of the wavelengths, *e.g.*, 940 mm, is almost absorbed by the water and thus cannot be detected by the event camera anymore.

Consequently, it is validated that our method allows to obtain the bispectral difference in a certain range where light at both the wavelengths is properly detected by the event camera. We will discuss cases where the frequency of the modulated signals is varied in Sec. 6.1.

5.3. Evaluations

Distance reconstruction We evaluate the performance of our method, compared with the existing method using the conventional camera [3]. Specifically, the accuracy and the range are evaluated through reconstructing a distance to the white board, as well as the validation. For comparison, we employ the iniVation DAVIS 346 including an active pixel sensor (APS) to capture a conventional brightness frame. In order to properly compare our method with the existing method, it is important to use the same silicon photodiode. We record events under the illumination modulated by 1 Hz triangle waves. And we also capture APS frames with multiple exposure times:2, 4, 8, 16, 32, 64, 128, 256, 512, and

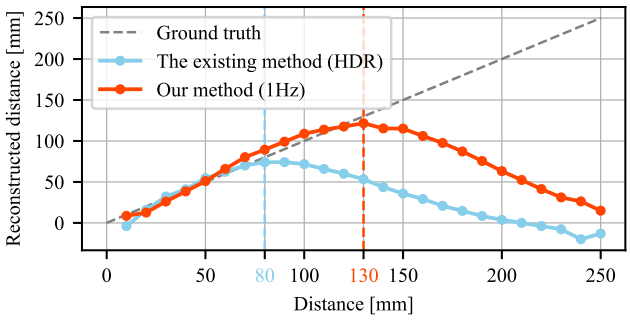

Figure 6: Experimental results of distance reconstruction in water.

1024 ms, to apply the HDR method [12] under the constant illumination with each of the wavelengths. The bispectral difference is reconstructed from the recorded events by Eq. (26) and calculated from the APS frames by Eq. (4). According to Eq. (28), the constant C has to be determined in a case of a known distance. However, selection of the known distance could affect the evaluation. Thus, we find the best constant C via a linear fitting. The reconstructed distances by both our and the existing methods are shown in Fig. 6. The gray dashed line denotes the ground truth, the red line the result by our method and the blue line that by the existing method. When we define a measurable range of distance as where an error is less than 15 mm, that range of our method is until 130 mm while that of the existing method is until 80 mm. The average error of our method in the measurable range and its standard deviation are 5.6 and 3.3 mm, while those of the existing method are 4.3 and 4.0 mm, respectively. The accuracy of both the methods is comparable but the measurable range of our method is way wider.

3D shape reconstruction The distance reconstruction can be performed for each pixel. Thus, it is possible to reconstruct a depth image. The frequency of the modulation signals is set to 1 Hz. In this experiment, the Prophesee EVK is employed because of its high spatial resolution. We also employ the conventional camera for comparison, because the Prophesee EVK does not have APS inside. Target objects are Golf Ball, Plastic Case and 3D Printed Stairs. Reconstructed depth images are shown in Fig. 7. The images from left to right are a photograph of the target object, the depth image reconstructed by ours and its 3D view, and the depth image reconstructed by the existing method and its 3D view, respectively. The reconstructed depth images are masked to reduce meaningless regions in the images and in the 3D view, smoothed surfaces of the depth are plotted. The depths are scaled in a range of 0 to 1. The experimental results show that the our method reconstructs the global 3D shape of the objects. The reconstructed shapes of the Golf Ball and the 3D Printed Stairs by our method

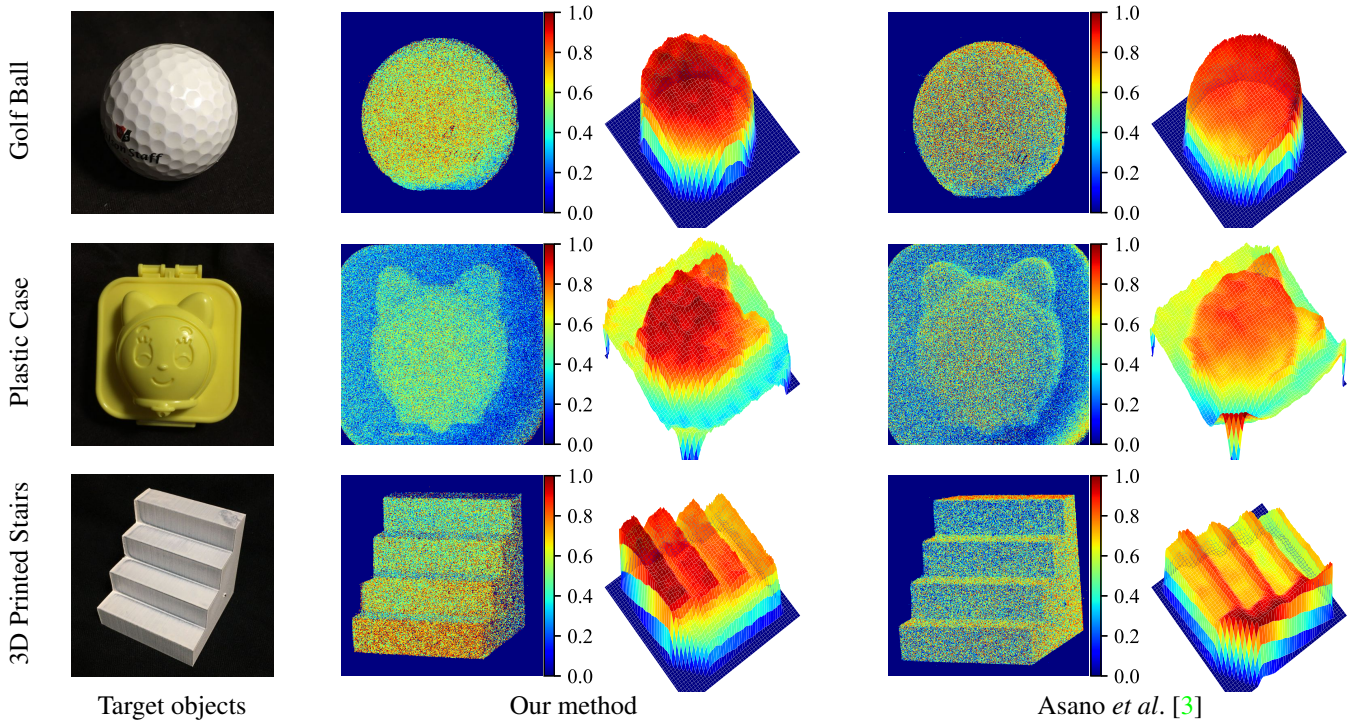

Figure 7: Experimental results of the depth image reconstruction in water.

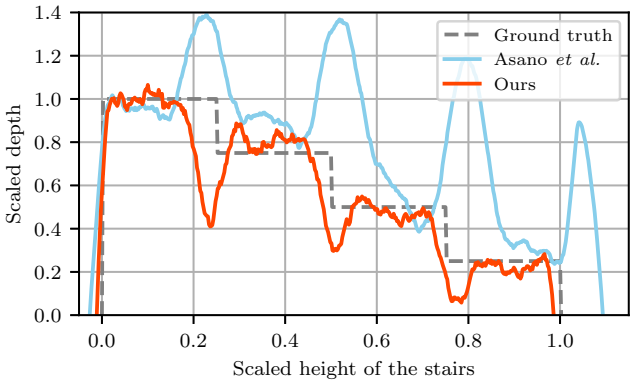

Figure 8: Cross-sections of the reconstructed 3D shape of the 3D Printed Stairs.

look more accurate than that by the existing method, while the existing method reconstructed a more detailed shape of the Plastic Case. In further comparison, we pick up the 3D Printed Stairs, because the geometry is known, to evaluate the cross-sections of the reconstructed 3D shape. The result shows that our method allows to reconstruct a better 3D shape than the existing method, as shown in Fig. 8.

Concentration reconstruction The bispectral difference can be used to reconstruct concentrations of a medium in mixture solution, as described in Eq. (6). The system is redesigned for the event camera to face the illumination module across a target medium, as shown in Fig. 9. The iniVation DAVIS 346 is employed in this experiment to compare with the existing method. The target medium is a mixture of water and soy sauce whose concentration is changed every $10\,\%$ from a range in 0 to $100\,\%$. The wavelengths of the light sources are changed into 637 and $850\,\mathrm{nm}$ (Thorlabs HL63142DG and L850P200, respectively) because the differential absorbance of soy sauce between the two wavelengths is large [50]. A plastic container whose geometry is known is used to store the medium, instead of the glass tank. Thus, the spectral calibration within the whole system is performed again. The bispectral difference is reconstructed using Eq. (26) and then the constant L is determined via a linear fitting, as well as the distance reconstruction. Reconstructed concentrations are shown in Fig. 9, where the gray line denotes the ground truth, the red line the result by our method and the blue line that by the existing method. When a measurable range of concentration is defined as where an error is less than $15\,\%$, the range of our method is until $70\,\%$ while that of the existing method is until $40\,\%$. The average error and its standard deviation by our method in the measurable range are $3.6\,\%$ and $4.0\,\%$, and those by the existing method are $5.2\,\%$ and $3.1\,\%$, respectively. The average error by our method is smaller than that by the existing method, and the measurable range of our method is way wider, as well as the evaluation in the distance reconstruction.

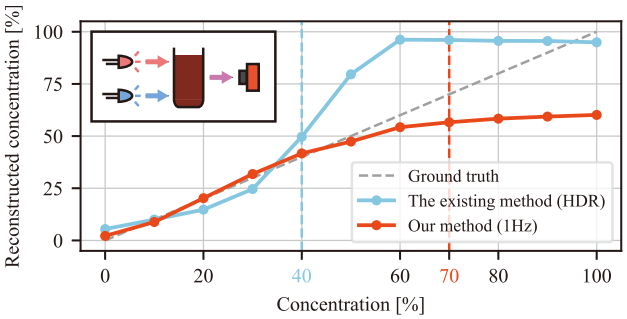

Figure 9: Experimental results of the concentration estimation of soy sauce.

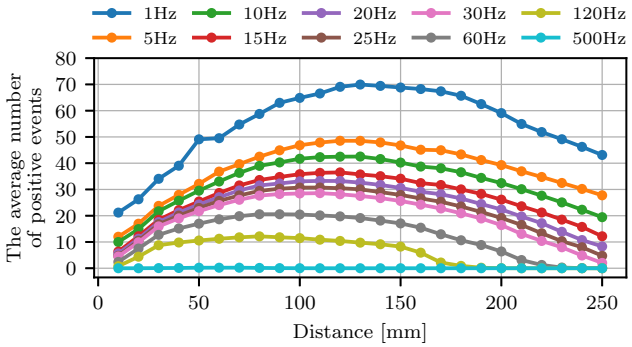

Figure 10: The average number of recorded positive events for various modulation frequencies. The white board is linearly translated every 10 mm.

6. Discussion and limitations

6.1. Frequency of modulation signals

The frequency of modulation signals seriously affects the performance of our method. A pixel inside a practical event camera has a dead time after triggering an event. During the dead time, no events can be triggered even if a temporal change in brightness is sufficiently large. The bandwidth of a practical event camera limits the number of recordable events per unit time, *i.e.*, an event rate. When brightness globally changes, a part of triggered events could be lost or delayed because of the limited bandwidth. Therefore, the number of recorded events by a practical event camera does not always match that by an ideal one. In the distance reconstruction, once the amplitude of a modulation signal, *e.g.*, the maximum intensity of light, is determined, the frequency is an important factor to decide the speed of change in brightness. In order to analyze the effect of the frequency, we demonstrate experiments using the Prophesee EVK, where the white board in water is linearly translated, as well as the validation. The frequency is changed in 1, 5, 10, 15, 20, 25, 30, 60, 120, and 500 Hz. The average numbers of recorded positive events for the various frequencies are shown in Fig. 10. Experimental results show that a lower frequency allows the event camera to more accurately record events. This is because a lower frequency makes the speed of change in brightness slower, which reduces the effect of the dead time and the limited event rate. Therefore, a lower frequency allows the performance of our method to be improved, while it takes a longer time to obtain the bispectral difference.

6.2. Limitations

There are three limitations on our method. First, the bandwidth of an event camera, *i.e.*, the event rate, limits the number of recordable events. Since the temporally modulated illumination in our method generates global changes in brightness, some events could be lost or delayed. To avoid this, we limited an illuminated region such that the event rate became around 10 Meps. This limitation could be resolved once an event camera with a higher event rate is developed, *i.e.*, iniVation DAVIS 346 (12 Meps) vs. Prophesee EVK (1066 Meps). Second, the current event cameras are unstable for photometry based analysis because of a large variance of the threshold h. The stability of measurements is important in photometry based analysis. The variance of stability is seen as the standard deviations in the validation, as shown in Fig. 5. This might be resolved by applying a statistical model. Third, we assume that a target scene is static. Since a dynamic scene itself triggers events, it is required to separate them from the events triggered by the modulated illumination. This is a future task to expand applications of photometry based analysis using event cameras.

7. Conclusion

In this paper, we proposed the event-based bispectral photometry to obtain a bispectral difference image using an event camera with temporally modulated illumination. We discovered the analogy between the bispectral photometry principle and the event generating mechanism in an event camera. Our design of the temporally modulated bispectral illumination allows to read out the bispectral difference directly as the number of events.

This paper verified the feasibility of the novel usage of event cameras in photometry based vision tasks. The advantages and limitations of event cameras were cleared up through the experiments. While event cameras have the features of HDR and high temporal resolution, variation in recorded events is significantly large. On the other hand, this could be a cue for statistical analysis in photometry based vision tasks, *e.g.*, photon density reconstruction. Event cameras are still an emerging device, which might have more potential to resolve the existing problems.

References

[1] Shigeru Ando and Akira Kimachi. Correlation image sensor: Two-dimensional matched detection of amplitude-modulated light. *IEEE Trans. on Electron Devices*, 50(10):2059–2066, Oct 2003.

[2] Alexander Andreopoulos, Hirak J. Kashyap, Tapan K. Nayak, Arnon Amir, and Myron D. Flickner. A Low Power, High Throughput, Fully Event-Based Stereo System. In *Proc. of IEEE Conf. on Computer Vision and Pattern Recognition*, pages 7532–7542, Salt Lake City, UT, USA, Jun 2018.

[3] Yuta Asano, Yinqiang Zheng, Ko Nishino, and Imari Sato. Depth Sensing by Near-Infrared Light Absorption in Water. *IEEE Trans. on Pattern Analysis and Machine Intelligence*, pages 1–12, Feb 2020.

[4] Patrick Bardow, Andrew J. Davison, and Stefan Leutenegger. Simultaneous optical flow and intensity estimation from an event camera. In *Proc. of IEEE Conf. on Computer Vision and Pattern Recognition*, pages 884–892, Las Vegas, NV, USA, Jun 2016.

[5] Samuel Bryner, Guillermo Gallego, Henri Rebecq, and Davide Scaramuzza. Event-based, Direct Camera Tracking from a Photometric 3D Map using Nonlinear Optimization. In *Proc. of IEEE Int'l Conf. on Robotics and Automation*, pages 1–8, Montreal, Canada, May 2019.

[6] Garland E. Busch, James G. Downward, Paul G. Gottschalk, Theodore B. Ladewski, and Charles D. Lysogorski. Electro-optical system for gauging surface profile deviations, Aug 1995.

[7] Clara Callenberg, Felix Heide, Gordon Wetzstein, and Matthias B. Hullin. Snapshot difference imaging using correlation time-of-flight sensors. In *ACM Trans. on Graphics*, volume 36, pages 1–11. Association for Computing Machinery, Nov 2017.

[8] Britton Chance. Rapid and sensitive spectrophotometry. III. A double beam apparatus. *Review of Scientific Instruments*, 22:634–638, 1951.

[9] Gregory Kevin Cohen. *Event-Based Feature Detection, Recognition and Classification*. Phd dissertation, University of Pierre et Marie Curie, 2017.

[10] R. T. H. Collis and P. B. Russell. Lidar measurement of particles and gases by elastic backscattering and differential absorption. In *Laser Monitoring of the Atmosphere. Topics in Applied Physics, vol 14*, pages 71–151. Springer, 1976.

[11] John C. Cowles. Theory of Dual-Wavelength Spectrophotometry for Turbid Samples. *Journal of the Optical Society of America*, 55(6):690–693, Jun 1965.

[12] Paul E. Debevec and Jitendra Malik. Recovering high dynamic range radiance maps from photographs. In *Proc. on SIGGRAPH '97*, page 369–378, 1997.

[13] R. Frouin, P. Y. Deschamps, and P. Lecomte. Determination from space of atmospheric total water vapor amounts by differential absorption near 940 nm: theory and airborne verification. *Journal of Applied Meteorology*, 29(6):448–460, 1990.

[14] Daniel Gehrig, Antonio Loquercio, Konstantinos G. Derpanis, and Davide Scaramuzza. End-to-End Learning of Representations for Asynchronous Event-Based Data. In *Proc. of IEEE Int'l Conf. on Computer Vision*, pages 5633–5643, Seoul, Korea, Oct 2019.

[15] Daniel Gehrig, Henri Rebecq, Guillermo Gallego, and Davide Scaramuzza. EKLT: Asynchronous photometric feature tracking using events and frames. *Int'l Journal of Computer Vision*, pages 1–18, 2018.

[16] S Gorog. *Ultraviolet-Visible Spectrophotometry in Pharmaceutical Analysis*. CRC Press, 1st editio edition, 1995.

[17] Reza Hajian and Ahmad Soltaninezhad. The spectrophotometric multicomponent analysis of a ternary mixture of paracetamol, aspirin, and caffeine by the double divisor-ratio spectra derivative method. *Journal of Spectroscopy*, 2013:1–7, 2013.

[18] Takeshi Kato, Hiroshi Kuzuya, and Toshiharu Nagatsu. A simple and sensitive assay for dopamine-β-hydroxylase activity by dual-wavelength spectrophotometry. *Biochemical Medicine*, 10(4):320 – 328, 1974.

[19] Hanme Kim, Stefan Leutenegger, and Andrew J. Davison. Real-Time 3D Reconstruction and 6-DoF Tracking with an Event Camera. In *Proc. of European Conference on Computer Vision*, pages 349–364, Amsterdam, Netherlands, Oct 2016.

[20] Akira Kimachi. Spectral matching imager using amplitude-modulation-coded multispectral light-emitting diode illumination. *Optical Engineering*, 43(4):975–985, Apr 2004.

[21] Grady J. Koch, Bruce W. Barnes, Mulugeta Petros, Jeffrey Y. Beyon, Farzin Amzajerdian, Jirong Yu, Richard E. Davis, Syed Ismail, Stephanie Vay, Michael J. Kavaya, and Upendra N. Singh. Coherent differential absorption lidar measurements of CO2. *Applied Optics*, 43(26):5092–5099, Sep 2004.

[22] Patrick Lichtsteiner, Christoph Posch, and Tobi Delbruck. A 128 × 128 120 dB 15 μs latency asynchronous temporal contrast vision sensor. *IEEE Journal of Solid-State Circuits*, 43(2):566–576, Feb 2008.

[23] E. Liljas. Multispectral classification of cloud, fog and haze. In R.A. Vaughan, editor, *Remote sensing applications in meteorology and climatology. NATO ASI Series (Series C: Mathematical and Physical Sciences), vol 201*, pages 301–319. Reidel; NATO ASI, Series C, 201, 1987.

[24] Ana I. Maqueda, Antonio Loquercio, Guillermo Gallego, Narciso Garcia, and Davide Scaramuzza. Event-Based Vision Meets Deep Learning on Steering Prediction for Self-Driving Cars. In *Proc. of IEEE Conf. on Computer Vision and Pattern Recognition*, pages 5419–5427, Salt Lake City, UT, USA, Jun 2018.

[25] Nathan Matsuda, Oliver Cossairt, and Mohit Gupta. MC3D: Motion Contrast 3D Scanning. In *Proc. of IEEE Int'l Conf. on Computational Photography*. Institute of Electrical and Electronics Engineers Inc., Jul 2015.

[26] Liang Mei, Peng Guan, and Zheng Kong. Remote sensing of atmospheric NO_2 by employing the continuous-wave differential absorption lidar technique. *Optics Express*, 25(20):A953–A962, Oct 2017.

[27] Anton Mitrokhin, Cornelia Fermuller, Chethan Parameshwara, and Yiannis Aloimonos. Event-Based Moving Object

Detection and Tracking. In *Proc. of IEEE/RSJ Int'l Conf. on Intelligent Robots and Systems*, pages 1–9, 2018.

[28] Ryohei Miyagawa and Takeo Kanade. CCD-based range-finding sensor. *IEEE Trans. on Electron Devices*, 44(10):1648–1652, 1997.

[29] Gottfried Munda, Christian Reinbacher, and Thomas Pock. Real-Time Intensity-Image Reconstruction for Event Cameras Using Manifold Regularisation. *Int'l Journal of Computer Vision*, 126(12):1381–1393, Dec 2018.

[30] Srinivasa G. Narasimhan, Shree K. Nayar, Bo Sun, and Sanjeev J. Koppal. Structured light in scattering media. In *Proc. of IEEE Int'l Conf. on Computer Vision*, volume I, pages 420–427, 2005.

[31] Richard J. Norman, Jeffrey C. Edberg, and Joseph W. Stucki. Determination of Nitrate in Soil Extracts by Dual-wavelength Ultraviolet Spectrophotometry. *Soil Science Society of America Journal*, 49(5):1182–1185, Sep 1985.

[32] Liyuan Pan, Cedric Scheerlinck, Xin Yu, Richard Hartley, Miaomiao Liu, and Yuchao Dai. Bringing a Blurry Frame Alive at High Frame-Rate with an Event Camera. In *Proc. of IEEE Conf. on Computer Vision and Pattern Recognition*, pages 6820–6829, Long Beach, CA, USA, Jun 2019.

[33] Michael Pircher, Erich Götzinger, Rainer Leitgeb, Adolf F. Fercher, and Christoph K. Hitzenberger. Measurement and imaging of water concentration in human cornea with differential absorption optical coherence tomography. *Optics Express*, 11(18):2190, Sep 2003.

[34] Ulrich Platt. Differential Optical Absorption Spectroscopy (DOAS). In Markus W. Sigrist, editor, *Air Monitoring by Spectroscopic Techniques. Chemical Analysis: A Series of Monographs on Analytical Chemistry and Its Applications*, pages 27–83. Wiley, 1994.

[35] Christoph Posch, Daniel Matolin, and Rainer Wohlgenannt. A QVGA 143 dB dynamic range frame-free PWM image sensor with lossless pixel-level video compression and time-domain CDS. *IEEE Journal of Solid-State Circuits*, 46(1):259–275, Jan 2011.

[36] Henri Rebecq, René Ranftl, Vladlen Koltun, and Davide Scaramuzza. Events-to-Video: Bringing Modern Computer Vision to Event Cameras. In *Proc. of IEEE Conf. on Computer Vision and Pattern Recognition*, pages 3857–3866, Long Beach, CA, USA, Jun 2019.

[37] Davidn W. Reynolds and Thomas H. Vonder Haar. A Bispectral Method for Cloud Parameter Determination. *Monthly Weather Review*, 105(4):446–457, Apr 1977.

[38] J. M. Schmitt, S. H. Xiang, and K. M. Yung. Differential absorption imaging with optical coherence tomography. *Journal of the Optical Society of America A*, 15(9):2288, Sep 1998.

[39] Stephan Schraml, Ahmed Nabil Belbachir, and Horst Bischof. Event-driven stereo matching for real-time 3D panoramic vision. In *Proc. of IEEE Conf. on Computer Vision and Pattern Recognition*, pages 466–474, Boston, MA, USA, Jun 2015.

[40] Yusuke Sekikawa, Kosuke Hara, and Hideo Saito. EventNet: Asynchronous Recursive Event Processing. In *Proc. of IEEE Conf. on Computer Vision and Pattern Recognition*, pages 3887–3896, Long Beach, CA, USA, Jun 2019.

[41] Shozo Shibata, Masamichi Furukawa, and Kazuo Goto. Dual-wavelength spectrophotometry. The determination of mixtures. *Analytica Chimica Acta*, 53(2):369–377, Feb 1971.

[42] Amos Sironi, Manuele Brambilla, Nicolas Bourdis, Xavier Lagorce, and Ryad Benosman. HATS: Histograms of Averaged Time Surfaces for Robust Event-Based Object Classification. In *Proc. of IEEE Conf. on Computer Vision and Pattern Recognition*, pages 1731–1740, Salt Lake City, UT, USA, Jun 2018.

[43] D. F. Swinehart. The Beer-Lambert law. *Journal of Chemical Education*, 39(7):333–335, 1962.

[44] Kenichiro Tanaka, Yasuhiro Mukaigawa, Takuya Funatomi, Hiroyuki Kubo, Yasuyuki Matsushita, and Yasushi Yagi. Material Classification from Time-of-Flight Distortions. *IEEE Trans. on Pattern Analysis and Machine Intelligence*, 41(12):2906–2918, Dec 2019.

[45] Kevin K. Tremper. Pulse Oximetry. *Chest*, 95(4):713–715, Apr 1989.

[46] Stepan Tulyakov, Martin Kiefel, Peter Gehler, and Michael Hirsch. Learning an event sequence embedding for dense event-based deep stereo. In *Proc. of IEEE Int'l Conf. on Computer Vision*, pages 1527–1537, Seoul, Korea, Oct 2019.

[47] Andrei B. Vakhtin, Kristen A. Peterson, William R. Wood, and Daniel J. Kane. Differential spectral interferometry: an imaging technique for biomedical applications. *Optics Letters*, 28(15):1332–1334, Aug 2003.

[48] Lin Wang, S. Mohammad Mostafavi I., Yo-Sung Ho, and Kuk-Jin Yoon. Event-based High Dynamic Range Image and Very High Frame Rate Video Generation using Conditional Generative Adversarial Networks. In *Proc. of IEEE Conf. on Computer Vision and Pattern Recognition*, pages 10081–10090, Long Beach, CA, USA, Jun 2019.

[49] Qiang Wang, Jun Chang, Wei Wei, Cunguang Zhu, and Changbin Tian. Dual-beam wavelength modulation spectroscopy for sensitive detection of water vapor. *Applied Physics B: Lasers and Optics*, 117(4):1015–1023, Nov 2014.

[50] Shuo Wang, Takehiro Tamura, Nobuyuki Kyouno, Xiaofang Liu, Han Zhang, Yoshinobu Akiyama, and Jie Yu Chen. Rapid detection of quality of Japanese fermented soy sauce using near-infrared spectroscopy. *Analytical Methods*, 12(18):2347–2354, May 2020.

[51] Hiroto Watanabe and Hideki Ohmori. Dual-wavelength spectrophotometric determination of cadmium with cadion. *Talanta*, 26(10):959–961, Oct 1979.

[52] Alex Zihao Zhu, Nikolay Atanasov, and Kostas Daniilidis. Event-based visual inertial odometry. In *Proc. of IEEE Conf. on Computer Vision and Pattern Recognition*, pages 5816–5824, Honolulu, HI, USA, Jul 2017.

[53] Alex Zihao Zhu, Yibo Chen, and Kostas Daniilidis. Realtime time synchronized event-based stereo. In *Proc. of European Conference on Computer Vision*, pages 438–452, Munich, Germarny, Sep 2018.